

Growth and Properties of Large Single Crystals of $\text{YBa}_2\text{Cu}_3\text{O}_{7-\delta}$ from $\text{BaCuO}_2/\text{CuO}$ Flux

B. A. Hunter, S. L. Town,^A D. N. Matthews, G. J. Russell and K. N. R. Taylor

School of Physics, University of New South Wales,
P.O. Box 1, Kensington, N.S.W. 2033, Australia.

^A ANSTO, Private Mail Bag 1, Menai, N.S.W. 2234, Australia.

Abstract

Large single crystals of $\text{YBa}_2\text{Cu}_3\text{O}_{7-\delta}$ have been grown using a $\text{BaCuO}_2/\text{CuO}$ flux whose composition lies close to the eutectic in the Y-Ba-Cu-O phase diagram. While the largest crystals produced were $\approx 20 \times 20 \times 0.7 \text{ mm}^3$, the average size of the remaining crystals was approximately $10 \times 10 \times 0.5 \text{ mm}^3$. These crystals, both as-grown and oxygen annealed, have been characterised using susceptibility measurements, optical and scanning microscopy and X-ray and neutron diffraction techniques.

1. Introduction

Numerous preparation routes for the growth of single crystals have been reported (Balestrino *et al.* 1987; Das *et al.* 1987; Hayashi *et al.* 1987; Hidaka *et al.* 1987; Kaiser *et al.* 1987; Scheel and Licci 1987; Schneemeyer *et al.* 1987; Takei *et al.* 1987; Takekawa and Iyi 1987; Keester *et al.* 1988; Taylor *et al.* 1988; Bosi *et al.* 1989; Sun *et al.* 1989; Taylor 1990; Watanabe 1990) since the discovery of the high temperature superconducting material $\text{YBa}_2\text{Cu}_3\text{O}_{7-\delta}$ (YBCO). Since this compound melts incongruently above 1000°C , depending on the oxygen partial pressure, it is not possible to grow crystals from the stoichiometric melt, and a flux growth method appears to offer the most successful route at the present time. With the continuing aim of producing large single crystals of this material, we have employed flux growth methods using both NaCl/KCl and $\text{BaCuO}_2/\text{CuO}$ fluxes.

This paper details the procedure we have used recently to produce repeatedly very large single crystals of YBCO using the more conventional $\text{BaCuO}_2/\text{CuO}$ flux where, for the flux proportions chosen, the flux had a melting temperature close to the eutectic temperature of the $\text{Y}_2\text{O}_3\text{-BaO-CuO}$ system. The as-grown crystals were not superconducting, however after 14 days of annealing in oxygen, superconductivity was observed. The crystals have been characterised using a number of techniques in the as-grown and annealed states.

2. Crystal Growth

The starting material for crystal growth was a BaCO_3/CuO mixture combined with finely ground, pre-sintered YBCO in the ratio $\text{BaCO}_3:\text{CuO}:\text{YBCO}$ of 50.0:51.83:6.8 by weight. The pre-sintered YBCO was produced by firing a stoichiometric mixture of Y_2O_3 , BaCO_3 and CuO at 930°C for 12 hours,

where k is Boltzmann's constant, c is the velocity of light, and

$$\eta_\nu = \frac{1}{\Omega_s} \int \{1 - \exp[-\tau_\nu(\theta, \phi)]\} d\theta d\phi. \quad (2)$$

The integral is evaluated over the solid angle of the source Ω_s , and $\tau_\nu(\theta, \phi)$ describes the two-dimensional distribution of optical depth at frequency ν . Coordinates (θ, ϕ) are a convenient Cartesian system.

Since $\tau_\nu(\theta, \phi) \geq 0$, we must have $0 \leq \eta_\nu \leq 1$. Referring to equation (1), we see that η_ν is a measure of the departure of the nebula from a black-body radiator. Note that if $\tau_\nu(\theta, \phi) \gg 1$ over Ω_s then $\eta_\nu \approx 1$, whereas if $\tau_\nu(\theta, \phi) \ll 1$ then $\eta_\nu \approx \langle \tau_\nu \rangle$, where the angle brackets denote averaging over Ω_s ,

$$\langle \tau_\nu \rangle = \frac{1}{\Omega_s} \int \tau_\nu(\theta, \phi) d\theta d\phi. \quad (3)$$

The critical frequency ν_c is defined at the intersection of the two regimes so that $\langle \tau_\nu \rangle = 1$ at $\nu = \nu_c$.

To apply equations (1) and (2) we need to know how $\tau_\nu(\theta, \phi)$ varies with ν , and this was given by Oster (1961) as

$$\tau_\nu(\theta, \phi) = \frac{8}{3(2\pi)^{1/2}} \frac{Z^2 e^6 \nu^{-2}}{c(mkT_e)^{3/2}} \ln \left[\frac{2(2kT_e)^{3/2}}{5\pi e^{-\gamma} m^{1/2} e^2 Z \nu} \right] E(\theta, \phi), \quad (4)$$

where Z ($=1$) is the atomic number, e and m are the electron charge and mass, γ ($=0.577$) is Euler's constant and $E(\theta, \phi)$ is the emission measure, defined as an integral of the product of the electron and ion densities along the line of sight through the nebula,

$$E(\theta, \phi) = \int N_e(\theta, \phi, z) N_i(\theta, \phi, z) dz. \quad (5)$$

Equation (4) is difficult to use since T_e and ν appear in the argument of the logarithm. A close approximation to it was given by Altenhoff *et al.* (1960),

$$\tau_\nu(\theta, \phi) = 0.082 Z^{1.9} T_e^{-1.35} \nu^{-2.10} E(\theta, \phi) \quad (6)$$

for T_e in K, ν in GHz, and E in pc cm^{-6} . As shown in Table 6 of Mezger and Henderson (1967), the error in equation (6) is mostly $<2\%$ in the range 300 MHz to 10 GHz for temperatures between 6000 and 14,000 K.

Since the frequency dependence of $\tau_\nu(\theta, \phi)$ is independent of the spatial distribution we may write

$$\tau_\nu(\theta, \phi) = \langle \tau_\nu \rangle \tau(\theta, \phi), \quad (7)$$

so that $\langle \tau(\theta, \phi) \rangle = 1$. Considering equations (1) and (2), we see that $\tau_\nu(\theta, \phi)$ enters into the determination of S_ν only through an integral over the surface of the nebula. This means that it is unnecessary to have the detailed two-dimensional information implicit in $\tau_\nu(\theta, \phi)$. For instance, if $\tau(\theta, \phi)$ is represented by a pixel map, the pixels within Ω_s may be rearranged spatially

without affecting the results. Alternatively, if the pixels were lined up in decreasing order of pixel height, a function $\tau(\Omega)$ of a solid angle variable Ω would be obtained, and this would contain all of the essential morphological information of $\tau(\theta, \phi)$. It is then natural to work in terms of

$$\omega = \frac{\Omega}{\Omega_s}. \tag{8}$$

Specifying $\tau(\omega)$ thus determines an infinite equivalence class of nebular morphologies which may look very different, but which are similar in terms of their radio continuum spectra. Equation (2) may be rewritten as

$$\eta_\nu = \int_0^1 \{1 - \exp[-\tau_\nu(\omega)]\} d\omega. \tag{9}$$

Likewise, combining equations (6) and (7) we have

$$\tau_\nu(\omega) = \langle \tau_\nu \rangle \tau(\omega) = \left(\frac{\nu}{\nu_c}\right)^{-2.1} \tau(\omega). \tag{10}$$

To compare the radio spectra of two models defined by $\tau_1(\omega)$ and $\tau_2(\omega)$, we might fix T_e , Ω_s , and ν_c at some arbitrary values and compute S_ν as a function of ν for each. The two spectra should differ from one another only where they turn over from being optically thick to optically thin. Alternatively, to avoid having to specify T_e and Ω_s , it is useful to normalise S_ν by dividing by s_ν , where

$$s_\nu = \frac{2kT_e\nu^2}{c^2} \Omega_s \langle \tau_\nu \rangle; \tag{11}$$

s_ν is effectively the extrapolation of the optically thin part of the radio spectrum to all frequencies. The modified spectrum \mathfrak{S}_ν , which is asymptotic to unity at high frequencies, is given by

$$\mathfrak{S}_\nu = \frac{S_\nu}{s_\nu} = \frac{\eta_\nu}{\langle \tau_\nu \rangle}; \tag{12}$$

\mathfrak{S}_ν might be thought of as a ‘*transparency*’, since it is unity in the optically thin regime and decreases towards zero with increasing optical depth.

If the value of ν_c is given, the spectrum of \mathfrak{S}_ν versus ν corresponding to $\tau(\omega)$ can be constructed through equations (9), (10) and (12). In turn, the observed radio flux densities can be fitted to this spectrum of \mathfrak{S}_ν by specifying s_0 , the value of s_ν at some standard frequency ν_0 . In practice, the best-fit values of ν_c and s_0 would be found via the least-squares or maximum likelihood methods of estimation. Note that approximate values of these two parameters could be measured directly from an adequately observed radio spectrum. The value of s_0 is determined by flux densities in the optically thin regime and these are often fairly accurate. On the other hand, the determination of ν_c relies also on observations at or below the turnover region of the spectrum, and these are usually fewer and less accurate. Once s_0 and ν_c are known and

experiments. The method we have adopted appears to be reproducible and we have now used this technique of crystal growth for a number of experiments, obtaining similar results in most cases.

In more recent crystal growth runs, the flux has been decanted onto an alumina firebrick located in the furnace at 930°C. The flux is rapidly absorbed into the porous brick, leaving many high quality crystals, which had nucleated in the liquid, on its surface. These are readily removed after cooling, and show no signs of contamination due to interaction with the alumina.

3. Results and Discussion

Scanning electron micrographs of several of these crystals generally show flat, smooth surfaces covered with extensive growth steps similar to those reported by ourselves and others (Scheel and Licci 1987; Kaiser *et al.* 1987; Taylor *et al.* 1988) and analysed in terms of growth mechanisms in this material by Sun *et al.* (1990). Energy dispersive X-ray analysis of the crystals confirmed the YBCO (123) composition with some evidence for Al contamination at concentrations of up to 1.5 At%. An X-ray diffraction pattern from the (001) face of an as-grown single crystal clearly reveals the tetragonal ($P4/mmm$) YBCO(123) phase, with cell parameters $a = b = 3.863(5) \text{ \AA}$, $c = 11.834(4) \text{ \AA}$, and no evidence of surface alumina contamination (Fig. 2). The oxygen content, calculated using the formula given by Wolf *et al.* (1988), was found to be $O_{6.3 \pm 0.1}$ (that is, $\delta = 0.7 \pm 0.1$) for the as-grown crystals. While optical polarimetric micrographs (see Fig. 3) again show the presence of growth steps, the absence of the twin related optical domain structure confirms the low oxygen content of these crystals.

Neutron diffraction measurements were made using the 2 TANA single crystal, four circle diffractometer at the HIFAR reactor, attached to the Australian Nuclear Science and Technology Organisation at Lucas Heights Research Laboratories, Sydney. Scans of the $(\Delta\omega, \Delta 2\theta)$ plane were made around the (200) reflection on an as-grown crystal at room temperature, using a wavelength of 1.237 \AA . These scans in $(\Delta\omega, \Delta 2\theta)$ space can be used to deconvolute a number of parameters, such as the mosaic spread in the crystal, the wavelength spread of the incident beam and the source divergence (Mathieson 1982). In our particular application it will only be used to differentiate between the tetragonal (single peak) and the orthorhombic (double peak for the crystal geometry studied) phases. A 2-D contour map of the intensity around this reflection is shown in Fig. 4a, in which only a single peak is visible, confirming that the sample is in the tetragonal phase; the observed spread in intensity along $\Delta\omega$ is due to the mosaic spread of the crystal (FWHM $\sim 0.23^\circ$). The same crystal was then heated in air, on the diffractometer, at $100^\circ\text{C}/\text{min}$ to 400°C and allowed to remain at this temperature for 3 days. The crystal was then cooled to room temperature at $20^\circ\text{C}/\text{min}$ and the previous measurement repeated. The same $(\Delta\omega, \Delta 2\theta)$ scan now clearly shows that the single peak has split, the two peaks being characteristic of twinning indicating that the sample has taken up oxygen and that a phase transition has occurred to the orthorhombic structure (Fig. 4b). These scans are similar to those done by McIntyre *et al.* (1988), except that due to the different crystal geometries we observe only two peaks instead of the four expected from that work. From these

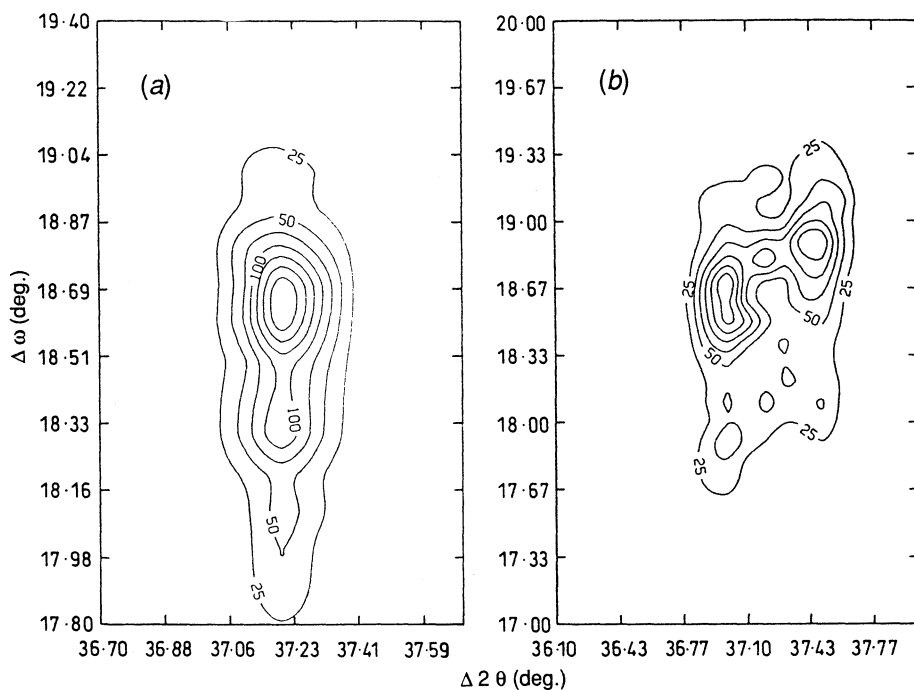


Fig. 4. (a) $(\Delta\omega, \Delta 2\theta)$ scans around the (200) reflection for an as-grown crystal, showing the tetragonal structure. (b) $(\Delta\omega, \Delta 2\theta)$ scans around the (200) reflection for the same crystal which was heated to 400°C for 3 days in air. Note that the single peak in (a) has now split and is characteristic of twinning and the orthorhombic structure.

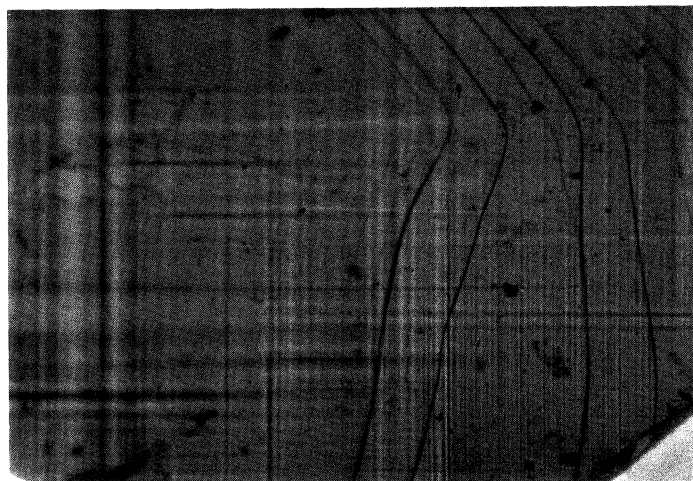


Fig. 5. Optical micrograph of the crystal surface region shown in Fig. 3, after annealing in flowing oxygen for 14 days at 550°C ($400\times$). Note the presence of twins.

contour plots we find the a - b splitting to correspond to an orthorhombicity, $(a-b)/(a+b) \approx 6.1 \times 10^{-3}$ and the angle of twinning to be $\alpha \approx 89.3^\circ$. The values of a and b were determined to be $3.882(5) \text{ \AA}$ and $3.835(4) \text{ \AA}$ respectively,

which is in good agreement with the study done by Brodt *et al.* (1990) on untwinned crystals of $\text{YBa}_2\text{Cu}_3\text{O}_{6.82}$.

Several crystals were further annealed at 550°C for 14 days in flowing oxygen at a pressure of one atmosphere, followed by cooling in oxygen to room temperature at approximately $10^\circ\text{C}/\text{hour}$. An X-ray diffraction pattern now showed the orthorhombic phase ($Pmmm$) with an oxygen content corresponding to $\delta = 0.2 \pm 0.1$. Optical micrographs, obtained after oxygenation, of the same crystal surface region shown in Fig. 3 revealed the presence of twins (Fig. 5). The a.c. susceptibility measurements were performed using a conventional balanced inductance bridge, with a drive field of 350 mOe at 257 Hz. The temperature variation of both the real (χ') and complex (χ'') components for a typical crystal is shown in Fig. 6. The magnetic transition showed an onset temperature of approximately 88 K, and as may be seen the transition is very broad with a number of discrete step-like changes in χ' that have equivalent loss peaks in χ'' . These results show that these large crystals are not fully oxygenated even after 14 days of oxygenation. The discrete loss peaks may be interpreted in terms of a number of ordered oxygen phases (Taylor *et al.* 1990). In view of the low oxygen diffusion coefficient for this material these results are not surprising, and the oxygenation is likely to be restricted to the surface regions of the crystal. The small aluminium contamination detected may also restrict the oxygen uptake, making it harder to produce a fully oxygenated crystal.

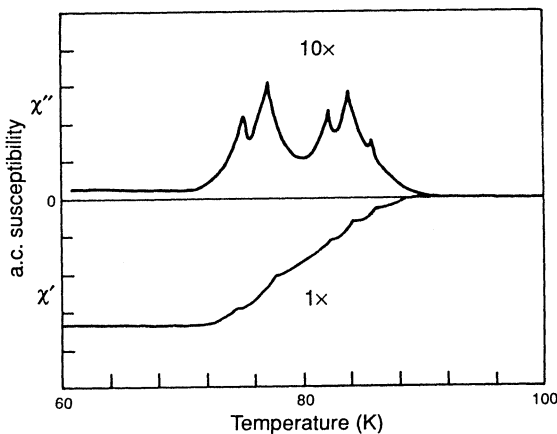


Fig. 6. The a.c. susceptibility, χ' and χ'' , for a crystal annealed at 550°C for 14 days in flowing oxygen at a pressure of one atmosphere. Note the presence of several transitions which we believe are associated with different ordered oxygen phases.

4. Conclusions

Conditions for the reproducible growth of large single crystals, $\approx 20 \times 20 \times 0.7 \text{ mm}^3$, of YBCO using a $\text{BaCuO}_2/\text{CuO}$ flux, have been detailed. The average size of the remaining crystals produced during a run were of the order $10 \times 10 \times 0.5 \text{ mm}^3$. The crystals were of regular shape, extremely smooth and

shiny but sometimes showed signs of inter-growth and residual flux on the surface. The crystals were also found to have a small aluminium contamination but this did not appear to have any significant effect on their properties. The as-grown crystals were found to have a low oxygen content, equivalent to $\delta = 0.7 \pm 0.1$, but this could be significantly increased by oxygenation at 550°C for 14 days, with the crystals then showing twinning and the suggestion of ordered oxygen phases.

Acknowledgments

One of us (B.A.H.) wishes to thank the Australian Institute of Nuclear Science and Engineering for a studentship during the course of this work.

References

- Balestrino, G., Barbanera, S., and Paroli, P. (1987). *J. Crystal Growth* **85**, 585.
- Bosi, S., Puzzer, T., Russell, G.J., Town, S.L., and Taylor, K.N.R. (1989). *J. Mat. Sci. Lett.* **8**, 497.
- Brodts, K., Fuess, H., Paulus, E.F., Assmus, W., and Kowalewski, J. (1990). *Acta Cryst. C* **46**, 354.
- Das, B.N., Toth, L.E., Singh, A.K., Bender, B., Osofsky, M., Pande, C.S., Koon, N.C., and Wolf, S. (1987). *J. Crystal Growth* **85**, 588.
- Hayashi, S., Komatsu, H., Inoue, T., Ono, T., Sasaki, K., Koike, Y., and Fukase, T. (1987). *Jpn J. Appl. Phys.* **26**, L1197.
- Hidaka, Y., Enomoto, Y., Suzuki, M., Oda, M., and Murakami, T. (1987). *J. Crystal Growth* **85**, 581.
- Kaiser, D.L., Holtzberg, F., Chisholm, M.F., and Worthington, T.K. (1987). *J. Crystal Growth* **85**, 593.
- Keester, K.L., Houssley, R.M., and Marshall, D.B. (1988). *J. Crystal Growth* **91**, 295.
- McIntyre, G.J., Renault, A., and Collin, G. (1988). *Phys. Rev. B* **37**, 5148.
- Mathieson, A.McL. (1982). *Acta Cryst. A* **38**, 378.
- Scheel, H.J., and Licci, F. (1987). *J. Crystal Growth* **85**, 607.
- Schneemeyer, L.F., Wasczak, J.V., Siegrist, T., Van Dover, R.B., Rupp, L.W., Batlogg, B., Cava, R.J. and Murphy, D.W. (1987). *Nature* **328**, 601.
- Sun, B.N., Boutellier, R., and Schmid, H. (1989). *Physica C* **157**, 189.
- Sun, B.N., Hartman, P., Woensdregt, C.F., and Schmid, H. (1990). *J. Crystal Growth* **100**, 605.
- Takei, H., Takeya, H., Iye, Y., Tamegai, T., and Sakai, F. (1987). *Jpn J. Appl. Phys.* **26**, L1425.
- Takekawa, S., and Iyi, N. (1987). *Jpn J. Appl. Phys.* **26**, L851.
- Taylor, K.N.R. (1990) 'In' *Studies of High Temperature Superconductors*, Vol. 6 (Ed. A. Narlikar), p. 1 (Nova: New York).
- Taylor, K.N.R., Cook, P.S., Puzzer, T., Matthews, D.N., Russell, G.J., and Goodman, P. (1988). *J. Crystal Growth* **88**, 541.
- Taylor, K.N.R., Russell, G.J., Bosi, S., Town, S.L., Hunter, B. A., and Darlington, C.N.W. (1990). *Proceedings Superconductivity Conference, Bangalore, Jan. 1990 to be published in Bull. Mater. Sci. (India)*.
- Watanabe, K. (1990). *J. Crystal Growth* **100**, 293.
- Wolf, T., Apfelstedt, I., Goldacker, W., Kupfer, H., and Flukiger, R. (1988). *Physica C* **153-155**, 351.

